JCI insight

Polycystin-1 regulates ARHGAP35-dependent centrosomal RhoA activation and ROCK signalling

Andrew J. Streets, … , Philipp P. Prosseda, Albert C.M. Ong

JCI Insight. 2020. https://doi.org/10.1172/jci.insight.135385.

Research In-Press Preview Genetics Nephrology

Graphical abstract

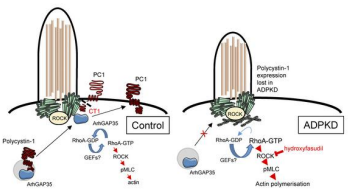

Polycystin-1 regulates ARHGAP35-dependent centrosomal RhoA activation and ROCK signalling

Andrew J Streets[1*], Philipp P. Prosseda[1], Albert CM Ong[1*]

[1]Kidney Genetics Group, Academic Nephrology Unit, Department of Infection, Immunity and Cardiovascular Disease, University of Sheffield Medical School, Sheffield, UK

*Address correspondence to:

Albert CM Ong or Andrew J Streets

Academic Nephrology Unit

Department of Infection, Immunity and Cardiovascular Disease

University of Sheffield Medical School

Beech Hill Road, Sheffield S10 2RX, UK

Tel: +44 114 215 9542

Fax: +44 114 271 3892

E-mail: a.ong@sheffield.ac.uk or a.j.streets@sheffield.ac.uk

The authors have declared that no conflict of interest exists

Abstract

Mutations in *PKD1* (encoding for Polycystin-1, PC1) are found in 80-85% of patients with ADPKD. We tested the hypothesis that changes in actin dynamics result from *PKD1* mutations through dysregulation of compartmentalised centrosomal RhoA signalling mediated by specific RhoGAP (ARHGAP) proteins resulting in the complex cellular cystic phenotype. Initial studies revealed that the actin cytoskeleton was highly disorganised in *PKD1* patient-derived cells and was associated with an increase in total and centrosomal RhoA activation and ROCK signalling. Using cilia length as a phenotypic readout for centrosomal RhoA activity, we identified ARHGAP5, 29, 35 as essential regulators of ciliation in normal human renal tubular cells. Importantly, a specific decrease in centrosomal ARHGAP35 was observed in *PKD1* null cells using a centrosome-targeted proximity ligation assay and by immunofluorescence labelling. Finally, we demonstrate that another ROCK inhibitor (hydroxyfasudil) reduced cyst expansion in both human *PKD1* 3D cyst assays and an inducible *Pkd1* mouse model. In summary, we report a novel interaction between PC1 and ARHGAP35 in the regulation of centrosomal RhoA activation and ROCK signalling. Targeting the RhoA/ROCK pathway inhibited cyst formation *in vitro* and *in vivo* indicating its relevance to ADPKD pathogenesis and for developing new therapies to inhibit cyst initiation.

Introduction

Autosomal dominant polycystic kidney disease (ADPKD) is the most common inherited cause of end-stage kidney failure in man (1). It has an estimated clinical prevalence of less than 1 in 2000 although its genetic prevalence could be higher due to many asymptomatic undiagnosed cases in the general population (2). Around 10% of patients on renal replacement therapy are due to ADPKD making it a disease of considerable personal, societal and economic impact. At present, only one drug, Tolvaptan, has been approved for use in man to slow disease progression (3).

Mutations in two genes, *PKD1* and *PKD2* account for the majority of cases (>90%) with ADPKD. In mutation-negative patients, a combination of mosaicism in *PKD1* or mutations in other cystic genes (*DNAJB11, GANAB*) have been detected although these still account for a small percentage of such cases (4, 5). *PKD1* encoding PC1 is the causative gene in 80-85% of patients making this the major ADPKD gene. It has also been recognised that other rarer cystic genes may exert their effects through alterations in the expression, processing or localisation of PC1 making an understanding of PC1 function central to the understanding and treatment of most forms of human PKD (6). This has however been a challenging task given the size, complexity and post-translational modifications of the protein (7).

The cellular phenotype of ADPKD is well described but is highly complex with alterations in many pathways reported. These include changes in proliferation, apoptosis, cell-cell and cell-matrix adhesion, differentiation, apicobasal polarity, fluid secretion, cilia function, directional migration and matrix deposition (7). In the majority of studies, it has been difficult to assign a specific phenotype to PC1 function. We tested the hypothesis that *PKD1* mutation leads to significant changes in actin cytoskeleton dynamics giving rise to several features of the cystic phenotype. In this study, we report that dysregulation of compartmentalised centrosomal RhoA

signalling mediated by a specific RhoGAP (ARHGAP35) leads to increased ROCK activation in *PKD1* mutant cells.

Results

Changes in actin cytoskeleton organisation are a striking feature of the ADPKD cellular phenotype

In preliminary studies, we observed that abnormalities in the actin cytoskeleton were a common feature of patient-derived *PKD1* cystic cell lines. Actin fibres appeared to be thicker, shorter and more disorganised in *PKD1* cells compared to non-cystic controls (Fig 1A-C). Structured illumination (3D-SIM) confocal images of phalloidin stained cells confirmed the general increase in cortical F-actin at the apical and basolateral surface, stress fibre formation and reduced cell height in a *PKD1* cell line (OX161) compared to a non-cystic control (UCL93) (Fig 1D, supplementary movies 1 and 2); in control cells, actin fibres were predominantly seen at the basal surface. In addition, we made the surprising observation that under conditions promoting optimal cilia formation (48h serum starvation), the percentage of ciliated cells as well as cilia length were reduced in *PKD1* cystic cells (Fig 1E, F, Fig S1A). These changes were not related to prolonged *in vitro* culture or immortalisation since a significant reduction in the cilia length and percentage of ciliated cells was also detected in nephrectomy tissue obtained from two *PKD1* patients (OX161 and SKI-001) compared to non-cystic patients (Fig S1B, D). Similar changes were confirmed in cystic kidney tissue from a *Pkd1* mouse model (8) (Fig S1C, E) excluding the possibility of secondary changes in late stage or end-stage disease in human tissues.

The cilia cellular phenotype is associated with increased actin polymerisation and PC1 deficiency

In view of the structural defects in actin organisation observed, we hypothesised that increased actin polymerisation could be the major underlying defect leading to shorter cilia in *PKD1*

cystic cells. Although the primary cilium is a microtubule-based organelle, it has been recognised that apical actin filaments are necessary to stabilise cilia formation by promoting centrosome migration, basal body docking and axoneme growth (9). These changes have been reported in rare ciliopathies such as Bardet-Biedel and Meckel syndromes (10, 11) although the role of actin in ciliogenesis in ADPKD has not been previously investigated. Strikingly, actin depolymerisation induced by cytochalasin D (1μM) increased cilia length in both normal and *PKD1* cystic cells to a similar degree (Fig 2A) linking the degree of actin polymerisation to cilia stabilisation. In contrast, a Rho-kinase (ROCK) inhibitor (Y-27632) restored cilia length in *PKD1* cells to that found in normal cells but had no effect on cilia length in normal cells (Fig 2B) implicating a mechanistic link between PC1 deficiency, RhoA activation and increased ROCK activity.

To confirm that this was the case, we generated *PKD1* null cells from the parental normal control human tubular cell line (UCL93) by CRISP/Cas9 mutagenesis. Three isogenic clones were selected for further study based on the absence of PC1 expression (Fig 2C). In early passage, we again observed a clear reduction in cilia length (Fig 2D, E) confirming a direct link to PC1 deficiency. In agreement with this, co-transfection of wild-type mCherry-PC1 (with wild-type PC2) into OX161 cells resulted in a partial rescue of the cilia phenotype; in contrast, no rescue was observed in cystic cells expressing a mutant mCherry-PC1-4211X truncation deleting most of the C-terminus (Fig 2 F-H). To investigate if PC2 was similarly implicated in this pathway, we generated *PKD2* null cells in the same line using the same strategy. *PKD2* null cells however had normal cilia lengths compared to the parental line (UCL93) indicating that the cilia phenotype is specific to PC1 and/or that PC2 plays a permissive but non-essential role (Fig S1F).

RhoA activation is increased in *PKD1* mutant or null cells and kidney tissues

To explore a potential mechanistic link between increased ROCK activity and PC1 deficiency, the activation of RhoA in disease cells and tissues was measured using a Rhotekin-RBD pull down assay designed to recognise GTP-RhoA. A significant increase in total GTP-RhoA was detectable in *PKD1* cystic cells compared to controls (Fig 3A) and confirmed in cystic kidneys of *Pkd1* mice (Fig 3B). Under conditions to promote cilia formation, we also observed a significant increase in total GTP-Cdc42 but not of GTP-Rac1 in *PKD1* cystic cells (Fig S2A-C). We also detected a significant increase in the phosphorylation of myosin light chain (MLC), a major downstream effector of ROCK which activates actin contraction and stabilisation, in *PKD1* null cells (Fig 3C).

Centrosomal RhoA activation is increased in *PKD1* cells and directly regulates cilia length

To exclude an additional role for Cdc42 or Rac1 in regulating cilia length, we next expressed dominant negative (DN) versions of each GTPase in *PKD1* cystic cells. As indicated, expression of DN RhoA (N19) but not DN Cdc42 (N17) or DN Rac1 (N17) increased cilia length in OX161 cells (Fig 3D). We hypothesised that apart from the total cellular increase in active GTP-RhoA, there was likely to be an increase in active RhoA at the centrosome or basal body compartment to account for the cilia phenotype in *PKD1* cells. Using a fluorescent active RhoA biosensor (12), we visualised significantly increased active RhoA in this compartment in *PKD1* cells compared to controls (Fig 3E). To confirm that an increase in active centrosome RhoA can result directly in shorter cilia, we exploited a rapamycin-inducible system to express constitutively active RhoA (Q63L) at the centrosome in control cells (Fig S3B). As shown, this resulted in significantly shorter cilia compared to non-induced cells (Fig 3F).

Knockdown of several centrosomal ARHGAPs decreased cilia length in control cells

The regulation of RhoA activity between the active GTP-bound state and the inactive GDP-bound state is mediated by ARHGEFs, which promote GTP binding and ARHGAPs which promote GTP hydrolysis (13). The increase in active RhoA at centrosomes which we observed in *PKD1* cells led us to hypothesise that a possible explanation could be loss of specific centrosomal ARHGAPs due to PC1 deficiency. Database and literature mining of several studies of the cilia/centrosome proteome and siRNA ciliogenesis screens identified 6 likely centrosomal ARHGAP proteins identified in at least two studies (Fig 4A) (14-20).

We therefore conducted a focussed siRNA screen on these 6 candidate ARHGAPs (ARHGAP 1, 5, 19, 21, 29, 35) in control cells (UCL93) achieving knockdown of >80% by QPCR (Fig S3A). Of note, knockdown of ARHGAP 5, 29 and 35 but not ARHGAP 1, 19 and 21 were found to significantly reduce ciliogenesis (Fig 4B, C).

Centrosomal ARHGAP35 localisation is reduced in PC1 null cells

The centrosomal localisation of ARHGAP 5, 29 and 35 in control UCL93 cells was experimentally confirmed using a BioID2 proximity ligation assay (PLA) linked to the centrosomal targeting PACT domain (Fig 4D, Fig S3C, D). Of interest, all three proteins were also detected using a second BioID2 PLA linked to the PC1 C-terminus (CT1) suggesting their close proximity to PC1 at centrosome and/or non-centrosome compartments (Fig 4D, Fig S3D).

To test whether the localisation of any of these centrosomal ARHGAPs could be regulated by PC1, we compared their centrosomal localisation in *PKD1* mutant (OX161) and *PKD1* null cells with isogenic control cells (UCL93) using the PACT-targeted BioID2 PLA. In the absence of PC1, a striking decrease in centrosome localisation of ARHGAP35 was noted (Fig 4E, F). We then confirmed the reduction in centrosomal ARHGAP35 in *PKD1* null cells by dual

immunofluorescence, with specific antibodies to γ-tubulin and ARHGAP35 (Fig 5A-C). In contrast, no significant change in centrosomal ARHGAP5 and ARHGAP29 was observed in the absence of PC1 (Fig S3E).

Co-immunoprecipitation of full-length epitope-tagged ARHGAP35 and PC1 expressed in HEK293 cells confirmed their direct interaction (Fig 5D). ARHGAP35 was shown to bind the PC1 C-terminus since it did not bind to a truncated PC1 mutant protein (CT1-R4227X) in GST-pull down assays (Fig 5E).

Rho kinase inhibition inhibits cyst growth *in vitro* and *in vivo*

The increase in total and centrosomal GTP-bound RhoA in *PKD1* deficient cells, the normalisation of cilia length by a ROCK inhibitor and the increased expression of pMLC, led us to conclude that ROCK might be a relevant therapeutic target in PKD1. We first tested the efficacy of a second ROCK inhibitor, hydroxyfasudil, in 3D cyst assays using a patient-derived *PKD1* cystic line (OX161). Hydroxyfasudil (1-30 μM, 7d) was associated with a significant decrease in cyst area confirming a likely link between the increased ROCK activity and cyst growth (Fig 6A).

Hydroxyfasudil is the major metabolite of the fasudil, one of the first ROCK inhibitors and has been shown to be effective in other preclinical models of kidney disease such as ischaemia-reperfusion injury, diabetic nephropathy and unilateral ureteric obstruction (21-23). We next tested the effectiveness of hydroxyfasudil in a tetracycline-inducible kidney-specific *Pkd1* mouse model (*Pax8*^{rtTA}*-TetO-Cre-Pkd1*$^{f/f}$) (24). Treatment with hydroxyfasudil (10mg/kg/day) from PN16-PN22 following kidney specific *Pkd1* deletion was well tolerated as reflected by changes in daily body weights (Fig 6B). After 7 days, the treated mice had reduced fractional kidney weights (2KW/BW) and fractional kidney cystic index compared to vehicle treated

controls (Fig 6C-E). Consistent with these changes, we observed a significant reduction in the proliferative index (Ki67 positive cells) and an increase in cilia length in treated animals (Fig 7A-D). The increase in cilia length seen in hydroxyfasudil-treated animals was also measurable when analysis was restricted to collecting duct-derived (DBA positive) cysts suggesting that the observed changes in cilia length following treatment were unlikely to be secondary to treatment-induced changes in the origin of individual cysts or a segment-specific effect (Fig 7E). In this model, few cysts were derived from proximal tubules as shown by the lack of LTA staining (Fig S4A). There was a non-significant decrease in BUN between vehicle and hydroxyfasudil-treated *Pkd1* animals after 7 days treatment; however, at this stage of disease, there was just a small increase in BUN between uninduced and induced *Pkd1* mice. Hydroxyfasudil did not alter BUN in the control (uninduced) animals (Fig S4B).

Discussion

In this study, we report that dramatic changes in the actin cytoskeleton are a striking feature of the ADPKD cystic cellular phenotype. An unexpected finding was of reduced ciliation, both in the number of ciliated cells and in cilia length in *PKD1* cystic cells, in *PKD1* and *Pkd1* cystic kidney tissue. To exclude the possibility of confounding factors such as genetic background, secondary genetic or epigenetic changes related to prolonged passage or cell immortalisation, we generated isogenic *PKD1* null cells by CRISP/Cas9 mutagenesis and found similar changes thus implicating this directly to PC1 expression. The molecular basis for this phenotype appears to be an increase in centrosome RhoA activation, leading to elevated ROCK activity and increased F-actin polymerisation and contractility. Using cilia length as a phenotypic readout for centrosomal RhoA activity, we identified three candidate ARHGAP proteins (ARHGAP5, 29, 35) as essential regulators of normal ciliation whose centrosome location had been reported

but whose function had not been previously defined. Nonetheless, we found that PC1 expression was only essential for the centrosomal localisation of ARHGAP35. We therefore conclude that the centrosome retention of ARHGAP5 and 29 are determined by their interaction with other proteins apart from PC1. A recent paper reported a glomerulocystic phenotype in an *Arhgap35* (p190A RhoGAP) mutant mouse model generated in an ENU mutagenesis screen (25). The amino-acid substitution (p.Leu1396Gln) leads to loss-of–function resulting in increased RhoA activity and reduced ciliogenesis (number and length) rescued by ROCK inhibition (25). Our findings confirm these results but extend them by providing the first evidence of a mechanistic link between ARHGAP35 and PC1 in cyst formation. It should be noted that homozygous *Arhgap35* mutant mice developed hypoplastic kidneys and heterozygous mice had normal kidneys and a low prevalence (<10%) of glomerular cysts. We conclude that a reduction in centrosomal PC1-ARHGAP35 interaction is likely to contribute to cyst formation in ADPKD but there could be compensation by other ARHGAPs such as ARHGAP5, 29 and others. Equally, other reported signalling pathways (centrosome and non-centrosome) likely contribute to cyst initiation and expansion in the ADPKD kidney. Although we have demonstrated that PC1 can bind to ARHGAP35, PC1 is mainly localised at the plasma and ciliary membrane while ARHGAP35 is localised to centrosome and non-centrosome (cell-cell, cell-matrix) compartments. It is plausible that both proteins could interact at the plasma membrane in non-centrosomal locations (see later). Nevertheless, since centrosomal ARHGAP35 localisation and/or retention is clearly dependent on PC1 (Figure 4), we speculate that this could relate to the trafficking and delivery of ARHGAP35 with PC1 to the centrosomes in the same vesicles (26) (27) and/or its retention at the centrosomes with the cleaved PC1 C-terminus (CT1) (28) (Figure 6).

The increase in RhoA activation in *PKD1* cells is probably not restricted to the centrosome compartment as reflected by the observed increase in total cellular GST-RhoA and pMLC

expression (Fig 3). The functional relevance of these findings to ADPKD pathogenesis was confirmed using the selective ROCK inhibitor hydroxyfasudil *in vitro* by 3D cyst assays using human-derived *PKD1* cystic cells and *in vivo* using a previously reported *Pkd1* inducible mouse model. It seems likely that the beneficial effect of ROCK inhibition in these models extends beyond the centrosomal actin sub-compartment; however it is possible that this could be the initiating signal for local RhoA activation which then spreads throughout the cell (Fig 8).

During the course of this study, two groups reported the beneficial effects of two other ROCK inhibitors in two neonatal *Pkd1* mouse models lending support to our findings (29, 30). In both studies, a functional link between increased RhoA/ROCK activity as a relevant upstream regulator of YAP/TAZ in ADPKD was reported. Nonetheless, our finding of a molecular link between PC1 and centrosomal ARHGAP35 is novel since neither study provided a direct mechanistic link to PC1. Our findings also imply that this is a very proximal or early change in cystic pathogenesis due to the molecular link between ARHGAP35 and PC1. Taken together, RhoA appears to be a common upstream molecule whose activity is altered by several abnormalities seen in ADPKD ie changes in cell-cell, cell-matrix and centrosome-cilia interactions.

Our results confirm the likely significance of the centrosome compartment both for cilia formation and as a major signalling node for regulating cellular function. Recent papers have shown that the centrosome is not only the main microtubule-organising centre but is also an actin filament-organising centre (31). The descriptions of several other centrosomal ARHGAPs and ARHGEFs from proteomic studies and a previous report of centrosomal ROCK localisation argue for the importance of fine-tuning compartmentalised RhoA/ROCK activity and consequent local actin dynamics both in health and disease (16) (32). The functional importance of each regulator, how they interact in local complexes and their relevance in ADPKD are important areas for future study. In addition, it is plausible that PC1 may regulate

the actin cytoskeleton in other cellular compartments where it has been localised (cell-cell junctions, cell-matrix contacts) (33, 34) through the recruitment or stabilisation of other ARHGAPs and/or ARHGEFs. In this context, it should be noted that ARHGAP35 has also been localised to both focal adhesions and cell-cell junctions in other cell types (35, 36).

Cdc42 has been reported to promote cilia formation through the localisation of the exocyst complex to the cilia base and kidney-specific cdc42 deletion is associated with cyst formation (37). Although we detected an increase in active Cdc42, expression of dominant-negative Cdc42 did not alter cilia length in our *Pkd1* cystic cells. These could reflect cell type or species differences. Nonetheless, Cdc42 activation could contribute to non-centrosomal changes in actin and microtubular dynamics in our cellular models, relevant to the cystic phenotype (38).

Centrosomal PC2 localisation has been reported in several studies though its function in this compartment is presently unclear. Notably, PC2 has been shown to bind to several centrosomal proteins including pericentrin and SCLT1, and may localise to the cilia base through binding the exosome protein Sec10/EXOC5 (37, 39, 40). It is also notable that PC2 has been shown to bind several actin-binding proteins (mDia1, actinin-4, filamin-A) which have been reported to regulate its channel activity (41-43). Nonetheless, PC2 null cells had normal cilia length in our study suggesting that the cilia phenotype is primarily related to changes in PC1 expression.

Our findings of reduced cilia length in the absence or mutation of PC1 are consistent with previous studies in both primary and immortalised *PKD1* cystic cells (44, 45). The current literature however has reports of normal, reduced or longer cilia length in association with PC1 deficiency. The first study of cilia length in $Pkd1^{del34}$ collecting duct-derived embryonic kidney cells (E15.5) reported ‘well developed’ cilia lengths (although formal measurements were not provided) in the context of loss of flow-induced cilia-mediated signalling (46). However, a later report using the same cells reported shorter cilia (with occasional long cilia) and

associated centrosomal abnormalities: in this study, increased expression of SIRT2 were causally linked to these changes (47). Conversely, *Pkd1* transgenic mice develop longer renal cilia in non-cystic tubules (48) although curiously, this phenotype has also been observed in either pre-cystic and/or cystic tissues and cells derived from several *Pkd1* deficient mice ie the $Pkd1^{RC/RC}$ hypomorphic mouse (49), *Pkd1* and *Pkd2* null embryonic (E15.5) kidney epithelial cells (50) and *Arl13b*-transgenic *Pkd1* mice (51). Since changes in PC1 dosage have been associated with variable changes in cilia length (none, reduced, increased) in different model systems, we conclude that this is not an essential feature of disease. The regulation of cilia length is complex and likely to be determined by multiple factors influencing both actin and microtubule-dependent mechanisms in disease (52). Differences between species, genetic background, segmental origin (44), differentiation and proliferative status (embryonic v adult-onset) (53), the presence of other functional cilia transgenes (eg *Arl13b*) (51) (54), organ involvement (kidney v liver) (49), inflammation (55), recovery from injury (56), senescence (57), mechanical forces (flow, stretch) or physical constraints (cell shape in 3D tissues) (58) could all be relevant modifying factors. A more systematic study examining these factors in other disease models will be needed. Alterations in cilia signalling could however be the common abnormality in all these models regardless of cilia length although there are currently opposing views on whether cilia themselves exert a negative effect on cell proliferation acting as a 'brake' on the cell cycle (59) or a positive effect through an unidentified 'cilia-dependent cyst-activating signal' (24) in the context of PKD.

ROCK inhibitors have been clinically approved for use in the treatment of glaucoma and vasospasm although their wider applications have been limited so far by systemic side-effects (60). Nonetheless, our results indicate that inhibition of the RhoA/ROCK axis in ADPKD is likely to be a major factor in cyst initiation and should stimulate the development of further therapeutic approaches in this area.

Materials and Methods

Materials

All chemicals were purchased from Sigma Chemical (Poole, Dorset, United Kingdom), unless otherwise stated. Plasmids were obtained through Addgene as indicated. The following antibodies were used in this study: PC1 (7e12), PC2 (g20), actin, ARHGAP5, ARHGAP29, myc, streptavidin, GST (Santa Cruz USA), ArhGAP35, MLC and pMLC (Cell Signalling, USA), Flag (Sigma, UK), RhoA, Cdc42 and Rac1 (Cytoskeleton Inc, USA), Arl13b (Proteintech).

Cell Lines

Non-cystic (UCL93, CL5, CL8, CL11) and cystic (OX161, OX938, SKI001, SKI002) human kidney epithelial cells were generated and cultured as previously described (61-63). Cilia formation was induced by serum starvation for 48h at 37°C

CrispR/Cas9 mutagenesis

UCL93 cells were transfected with pSpCas9(BB)-2A-Puro(PX459) V2.0 (pSpCas9n(BB)-2A-Puro (PX462) V2.0 (gift of Feng Zhang, Addgene plasmid #6298) (64) containing a gDNA targeting the first exon of *PKD1* (5'-CACCGCGCCGGGCGCTGGGCCGCAG) or the first exon of *PKD2* (5' CACCGCGTGGAGCCGCGATAACCC). Positive clones were selected for puromycin resistance followed by limiting dilution. Mutations were then validated by genomic DNA sequencing and western blotting using specific antibodies to PC1 (7e12) and PC2 (1A11) (65, 66).

Transfections

Cells were transfected using Lipofectamine 3000 (Life Technologies) for 48h prior to the cell assays. For siRNA knockdown assays, cells were transfected with negative control or specific ARHGAP siRNAs (SmartPool, Dharmacon, USA) using RNAimax (Life Technologies). siRNA knockdown was confirmed by qPCR using specific Taqman probes.

Western blotting and immunoprecipitation

Total cell lysates were prepared and processed for immunoprecipitation and Western blotting as described (67). Cells were solubilized in detergent lysis buffer (50 mM Tris, 0.14 M NaCl, 1% Triton X-100, and 0.5% NP40) supplemented with Complete protease inhibitors and PhosStop phosphatase inhibitors (Roche Diagnostics, Mannheim, Germany). Immunoprecipitation and GST pulldown assays were performed as previously described (26), ECL detection and quantification using a Biorad Chemidoc XRS+ system running Image Lab automated image capture and analysis software. All quantification was carried out on non-saturated bands as determined by the software from 3 independent experiments.

BioID proximity assay

A common centrosomal targeting domain identified from pericentrin and AKAP450 (PACT) (68) or the C-terminal domain of PC1 (CT1) was cloned into myc-BioID2-MCS (myc-BioID2-MCS (gift of Kyle Roux, Addgene plasmid # 74223) (69). Following transfection, cells were incubated with 50 μM biotin (Sigma #B4501) overnight. Lysates were prepared as described and incubated with 50 μl Dynabeads MyOne Streptavidin C1 for 4h. The beads were washed

6 times with lysis buffer, bound proteins eluted, separated by SDS-PAGE prior to analysis by immunoblotting with specific ARHGAP primary antibodies.

Active RhoA, Cdc42 and Rac1 pulldown assays

Levels of GTP-bound RhoA were determined using a Rhotekin-RBD bead pull-down assay. Levels of GTP bound Cdc42 or Rac1 were determined by PAK-PBD beads pull down assays (Cytoskeleton, Inc, USA) as described. GTP-γ and GDP treated cell lysates were used as positive and negative controls respectively. Samples were separated by SDS-PAGE and analysed by immunoblotting with RhoA, Cdc42 or Rac1 antibodies.

Rho-GTPase Biosensor

The active RhoA biosensor GFP-rGBD (gift of William Bement, Addgene plasmid # 26732) (12) was transfected into UCL93 or OX161 cells. Following serum starvation to induce cilia formation, the proportion of cells localising GFP-rGBD at the cilia base was quantified.

Polycystin rescue experiment

UCL93 and OX161 cells were transfected using Amaxa electroporation (program W-01) with CFP-PC2 (27) and mCherry-PC1 or mCherry-PC1-4211X (gifts of Peter Harris, Mayo Clinic) (70). Following transfection, cells were serum starved for 48h at 37°C to induce cilia formation. Cilia were stained with Arl13b and measurements were performed on mCherry-PC1 transfected cells with an Olympus Imaging Systems inverted IX-71 microscope set to capture cellular fluorescence images with a CCD camera (Hamamatsu), driven by Simple PCI software (C Imaging Systems).

Rapamycin induced centrosome translocation

YF-RhoA (CA) (Addgene plasmid # 20153) and Lyn11-targeted FRB (LDR) (Addgene plasmid #20147) were gifts of Tobias Meyer, Stanford (71). The PACT centrosomal targeting domain was cloned into LDR replacing the Lyn11 plasma membrane targeting domain. UCL93 cells were transfected with YF-RhoA (CA) and PACT-FRB-HA. Translocation of YF-RhoA to the centrosome was induced 24h later by the addition of 10µm rapamycin (Calbiochem)for 10 min, washed followed by serum starvation for 48h at 37°C to induce cilia formation. Cilia were stained with Arl13b and measurements were performed on an Olympus Imaging Systems inverted IX-71 microscope set to capture cellular fluorescence images with a CCD camera (Hamamatsu), driven by Simple PCI software (C Imaging Systems).

Immunofluorescence staining

Immunofluorescence staining was performed as previously described (26, 27). Primary cilia were visualised using an antibody to Arl13b (Proteintech). HA and myc epitope tagged proteins were detected with anti-HA and anti-myc polyclonal antibodies (Santa Cruz, USA) and Alexa Fluor 488 or 594 secondary antibodies (Invitrogen, USA). F-actin was detected using Rhodamine-Phalloidin (Invitrogen, USA). For mouse tissue, serial sections were dewaxed and rehydrated and antigen retrieval was carried out using Tris-EDTA (pH 9). DBA and LTA lectin positive cysts were identified using FITC conjugated lectins (Vector Labs, USA). Slides were viewed using an Imaging Systems inverted IX71 microscope (Olympus, Tokyo, Japan) configured for multifluorescence image capture. Images were acquired using SimplePCI imaging software (Compix, Hamamatsu, PA). For cilia length measurements, ImageJ analysis software (NIH) was used to measure >100 cilia in at least 3 independent experiments.

Cytochalasin D and the ROCK inhibitor Y-27632 were added to cells at the indicated concentrations for 3h prior to cilia length measurement. Super resolution microscopy was carried out on a DeltaVision/ GE OMX optical microscope (version 4) for structured illumination (3D-SIM) and analysed using Imaris image analysis software (Bitplane).

Matrigel 3D cyst assays

3D matrigel cyst assays were performed as previously described (62). In brief, OX161/C1 cells ($1x10^5$/well) were mixed with 70 µl Matrigel (Becton Dickinson, UK), plated into 96 well plates in triplicate and incubated for 30 min at 37°C to facilitate gel formation. Cells were then cultured for 12d in the presence of hydroxyfasudil (Tocris, UK). Media was replaced every 2 d. The average cyst area was calculated by measuring cyst areas in individual wells on day 12. At least 65 cysts were measured in triplicate wells at each time-point.

Effect of hydroxyfasudil in vivo

Pkd1 deletion was induced by doxycycline injections at post-natal day (PN) 13-15 in tetracycline-inducible kidney-specific *Pkd1* mice (*Pax8^{rtTA}-TetO-Cre-Pkd1$^{f/f}$*) (72). Experimental animals were injected IP with hydroxyfasudil (10mg/kg/day) or vehicle (sterile water) for 7 d from PN16. After sacrifice following a Schedule 1 method, blood and tissues were rapidly collected. Blood was collected and centrifuged at 2,000 x g for 10 minutes to collect serum that was quickly snap frozen in liquid nitrogen and stored at -80 °C until further analysis. Each kidney was cut transversally into 4 pieces. The top and bottom sections were snap frozen for biochemical analysis while the middle section was embedded in cry-M-bed solution (Wolflabs) or immersed in 10% Neutral Buffered Formalin (Sigma-Aldrich) for histological analysis. Following termination at PN23, terminal 2KW/BW was calculated and

tissue sections analysed for cystic index, cilia length (Arl13b) and proliferation index (Ki67). Serum blood urea nitrogen (BUN) measurements were carried out by the Department of Clinical Chemistry at the Sheffield Children's Hospital Foundation Trust.

Statistical Analysis

Data are presented as mean values ± SEM. Student's t test (two tailed) and one way Anova corrected for multiple comparisons were used for statistical analysis with a p value of <0.05 indicating statistical significance.

Study Approval

Animal studies were approved by the University of Sheffield Medical School and carried out under Home Office licence PF2A3AD69. A tetracycline-inducible kidney-specific *Pkd1* mouse model (*Pax8*^{rtTA}*-TetO-Cre-Pkd1*$^{f/f}$) on a C57/BL6 background was obtained from the Baltimore PKD Centre (kind gift of the late David Huso).

Author Contributions

PPP conducted experiments, acquired data and analysed data. AJS conducted experiments, designed research studies, acquired and analysed data and helped to write the manuscript. AO obtained funding, designed research studies, analysed data and wrote the manuscript.

Acknowledgements

This study was supported by grants from Kidney Research UK (ST3/2011) and the Sheffield Kidney Research Foundation. We thank Lisa Chang and Maya Boudiffa for expert technical assistance.

References

1. Ong AC, Devuyst O, Knebelmann B, Walz G, and Diseases E-EWGfIK. Autosomal dominant polycystic kidney disease: the changing face of clinical management. *Lancet.* 2015;385(9981):1993-2002.
2. Lanktree MB, Haghighi A, Guiard E, Iliuta IA, Song X, Harris PC, et al. Prevalence Estimates of Polycystic Kidney and Liver Disease by Population Sequencing. *J Am Soc Nephrol.* 2018;29(10):2593-600.
3. Torres VE, Chapman AB, Devuyst O, Gansevoort RT, Perrone RD, Koch G, et al. Tolvaptan in Later-Stage Autosomal Dominant Polycystic Kidney Disease. *N Engl J Med.* 2017;377(20):1930-42.
4. Cornec-Le Gall E, Olson RJ, Besse W, Heyer CM, Gainullin VG, Smith JM, et al. Monoallelic Mutations to DNAJB11 Cause Atypical Autosomal-Dominant Polycystic Kidney Disease. *Am J Hum Genet.* 2018;102(5):832-44.
5. Porath B, Gainullin VG, Cornec-Le Gall E, Dillinger EK, Heyer CM, Hopp K, et al. Mutations in GANAB, Encoding the Glucosidase IIalpha Subunit, Cause Autosomal-Dominant Polycystic Kidney and Liver Disease. *Am J Hum Genet.* 2016;98(6):1193-207.
6. Ong ACM. Making sense of polycystic kidney disease. *Lancet.* 2017;389(10081):1780-2.
7. Ong AC, and Harris PC. A polycystin-centric view of cyst formation and disease: the polycystins revisited. *Kidney Int.* 2015;88(4):699-710.
8. Lantinga-van Leeuwen IS, Leonhard WN, van der Wal A, Breuning MH, de Heer E, and Peters DJ. Kidney-specific inactivation of the Pkd1 gene induces rapid cyst formation in developing kidneys and a slow onset of disease in adult mice. *Hum Mol Genet.* 2007;16(24):3188-96.
9. Pan J, You Y, Huang T, and Brody SL. RhoA-mediated apical actin enrichment is required for ciliogenesis and promoted by Foxj1. *J Cell Sci.* 2007;120(Pt 11):1868-76.
10. Dawe HR, Adams M, Wheway G, Szymanska K, Logan CV, Noegel AA, et al. Nesprin-2 interacts with meckelin and mediates ciliogenesis via remodelling of the actin cytoskeleton. *J Cell Sci.* 2009;122(Pt 15):2716-26.
11. Hernandez-Hernandez V, Pravincumar P, Diaz-Font A, May-Simera H, Jenkins D, Knight M, et al. Bardet-Biedl syndrome proteins control the cilia length through regulation of actin polymerization. *Hum Mol Genet.* 2013;22(19):3858-68.
12. Benink HA, and Bement WM. Concentric zones of active RhoA and Cdc42 around single cell wounds. *J Cell Biol.* 2005;168(3):429-39.
13. Hodge RG, and Ridley AJ. Regulating Rho GTPases and their regulators. *Nat Rev Mol Cell Biol.* 2016;17(8):496-510.
14. Kim J, Lee JE, Heynen-Genel S, Suyama E, Ono K, Lee K, et al. Functional genomic screen for modulators of ciliogenesis and cilium length. *Nature.* 2010;464(7291):1048-51.
15. Wheway G, Schmidts M, Mans DA, Szymanska K, Nguyen TT, Racher H, et al. An siRNA-based functional genomics screen for the identification of regulators of ciliogenesis and ciliopathy genes. *Nat Cell Biol.* 2015;17(8):1074-87.
16. Boldt K, van Reeuwijk J, Lu Q, Koutroumpas K, Nguyen TM, Texier Y, et al. An organelle-specific protein landscape identifies novel diseases and molecular mechanisms. *Nat Commun.* 2016;7:11491.
17. Mick DU, Rodrigues RB, Leib RD, Adams CM, Chien AS, Gygi SP, et al. Proteomics of Primary Cilia by Proximity Labeling. *Dev Cell.* 2015;35(4):497-512.
18. Ishikawa H, Thompson J, Yates JR, 3rd, and Marshall WF. Proteomic analysis of mammalian primary cilia. *Curr Biol.* 2012;22(5):414-9.
19. Roosing S, Hofree M, Kim S, Scott E, Copeland B, Romani M, et al. Functional genome-wide siRNA screen identifies KIAA0586 as mutated in Joubert syndrome. *eLife.* 2015;4:e06602.
20. Gupta GD, Coyaud E, Goncalves J, Mojarad BA, Liu Y, Wu Q, et al. A Dynamic Protein Interaction Landscape of the Human Centrosome-Cilium Interface. *Cell.* 2015;163(6):1484-99.

21. Baba I, Egi Y, Utsumi H, Kakimoto T, and Suzuki K. Inhibitory effects of fasudil on renal interstitial fibrosis induced by unilateral ureteral obstruction. *Mol Med Rep.* 2015;12(6):8010-20.
22. Kentrup D, Reuter S, Schnockel U, Grabner A, Edemir B, Pavenstadt H, et al. Hydroxyfasudil-mediated inhibition of ROCK1 and ROCK2 improves kidney function in rat renal acute ischemia-reperfusion injury. *PLoS One.* 2011;6(10):e26419.
23. Peng H, Li Y, Wang C, Zhang J, Chen Y, Chen W, et al. ROCK1 Induces Endothelial-to-Mesenchymal Transition in Glomeruli to Aggravate Albuminuria in Diabetic Nephropathy. *Sci Rep.* 2016;6:20304.
24. Ma M, Tian X, Igarashi P, Pazour GJ, and Somlo S. Loss of cilia suppresses cyst growth in genetic models of autosomal dominant polycystic kidney disease. *Nature genetics.* 2013;45(9):1004-12.
25. Stewart K, Gaitan Y, Shafer ME, Aoudjit L, Hu D, Sharma R, et al. A Point Mutation in p190A RhoGAP Affects Ciliogenesis and Leads to Glomerulocystic Kidney Defects. *PLoS Genet.* 2016;12(2):e1005785.
26. Feng S, Streets AJ, Nesin V, Tran U, Nie H, Onopiuk M, et al. The Sorting Nexin 3 Retromer Pathway Regulates the Cell Surface Localization and Activity of a Wnt-Activated Polycystin Channel Complex. *J Am Soc Nephrol.* 2017;28(10):2973-84.
27. Xu Y, Streets AJ, Hounslow AM, Tran U, Jean-Alphonse F, Needham AJ, et al. The Polycystin-1, Lipoxygenase, and alpha-Toxin Domain Regulates Polycystin-1 Trafficking. *J Am Soc Nephrol.* 2016;27(4):1159-73.
28. Bertuccio CA, Chapin HC, Cai Y, Mistry K, Chauvet V, Somlo S, et al. Polycystin-1 C-terminal Cleavage Is Modulated by Polycystin-2 Expression. *J Biol Chem.* 2009;284(31):21011-26.
29. Cai J, Song X, Wang W, Watnick T, Pei Y, Qian F, et al. A RhoA-YAP-c-Myc signaling axis promotes the development of polycystic kidney disease. *Genes Dev.* 2018;32(11-12):781-93.
30. Nigro EA, Distefano G, Chiaravalli M, Matafora V, Castelli M, Pesenti Gritti A, et al. Polycystin-1 Regulates Actomyosin Contraction and the Cellular Response to Extracellular Stiffness. *Sci Rep.* 2019;9(1):16640.
31. Farina F, Gaillard J, Guerin C, Coute Y, Sillibourne J, Blanchoin L, et al. The centrosome is an actin-organizing centre. *Nat Cell Biol.* 2016;18(1):65-75.
32. Chevrier V, Piel M, Collomb N, Saoudi Y, Frank R, Paintrand M, et al. The Rho-associated protein kinase p160ROCK is required for centrosome positioning. *J Cell Biol.* 2002;157(5):807-17.
33. Streets AJ, Wagner BE, Harris PC, Ward CJ, and Ong AC. Homophilic and heterophilic polycystin 1 interactions regulate E-cadherin recruitment and junction assembly in MDCK cells. *J Cell Sci.* 2009;122(Pt 9):1410-7.
34. Wilson PD, Geng L, Li X, and Burrow CR. The PKD1 gene product, "polycystin-1," is a tyrosine-phosphorylated protein that colocalizes with alpha2beta1-integrin in focal clusters in adherent renal epithelia. *Lab Invest.* 1999;79(10):1311-23.
35. Bradley WD, Hernandez SE, Settleman J, and Koleske AJ. Integrin signaling through Arg activates p190RhoGAP by promoting its binding to p120RasGAP and recruitment to the membrane. *Mol Biol Cell.* 2006;17(11):4827-36.
36. Wildenberg GA, Dohn MR, Carnahan RH, Davis MA, Lobdell NA, Settleman J, et al. p120-catenin and p190RhoGAP regulate cell-cell adhesion by coordinating antagonism between Rac and Rho. *Cell.* 2006;127(5):1027-39.
37. Choi SY, Chacon-Heszele MF, Huang L, McKenna S, Wilson FP, Zuo X, et al. Cdc42 deficiency causes ciliary abnormalities and cystic kidneys. *J Am Soc Nephrol.* 2013;24(9):1435-50.
38. Cau J, and Hall A. Cdc42 controls the polarity of the actin and microtubule cytoskeletons through two distinct signal transduction pathways. *J Cell Sci.* 2005;118(Pt 12):2579-87.

39. Jurczyk A, Gromley A, Redick S, San Agustin J, Witman G, Pazour GJ, et al. Pericentrin forms a complex with intraflagellar transport proteins and polycystin-2 and is required for primary cilia assembly. *J Cell Biol.* 2004;166(5):637-43.
40. Li J, Lu D, Liu H, Williams BO, Overbeek PA, Lee B, et al. Sclt1 deficiency causes cystic kidney by activating ERK and STAT3 signaling. *Hum Mol Genet.* 2017;26(15):2949-60.
41. Bai CX, Kim S, Li WP, Streets AJ, Ong AC, and Tsiokas L. Activation of TRPP2 through mDia1-dependent voltage gating. *EMBO J.* 2008;27(9):1345-56.
42. Li Q, Montalbetti N, Shen PY, Dai XQ, Cheeseman CI, Karpinski E, et al. Alpha-actinin associates with polycystin-2 and regulates its channel activity. *Hum Mol Genet.* 2005;14(12):1587-603.
43. Wang Q, Zheng W, Wang Z, Yang J, Hussein S, Tang J, et al. Filamin-a increases the stability and plasma membrane expression of polycystin-2. *PLoS One.* 2015;10(4):e0123018.
44. Xu C, Shmukler BE, Nishimura K, Kaczmarek E, Rossetti S, Harris PC, et al. Attenuated, flow-induced ATP release contributes to absence of flow-sensitive, purinergic Cai2+ signaling in human ADPKD cyst epithelial cells. *Am J Physiol Renal Physiol.* 2009;296(6):F1464-76.
45. Xu C, Rossetti S, Jiang L, Harris PC, Brown-Glaberman U, Wandinger-Ness A, et al. Human ADPKD primary cyst epithelial cells with a novel, single codon deletion in the PKD1 gene exhibit defective ciliary polycystin localization and loss of flow-induced Ca2+ signaling. *Am J Physiol Renal Physiol.* 2007;292(3):F930-45.
46. Nauli SM, Alenghat FJ, Luo Y, Williams E, Vassilev P, Li X, et al. Polycystins 1 and 2 mediate mechanosensation in the primary cilium of kidney cells. *Nat Genet.* 2003;33(2):129-37.
47. Zhou X, Fan LX, Li K, Ramchandran R, Calvet JP, and Li X. SIRT2 regulates ciliogenesis and contributes to abnormal centrosome amplification caused by loss of polycystin-1. *Hum Mol Genet.* 2014;23(6):1644-55.
48. Kurbegovic A, Cote O, Couillard M, Ward CJ, Harris PC, and Trudel M. Pkd1 transgenic mice: adult model of polycystic kidney disease with extrarenal and renal phenotypes. *Hum Mol Genet.* 2010;19(7):1174-89.
49. Hopp K, Ward CJ, Hommerding CJ, Nasr SH, Tuan HF, Gainullin VG, et al. Functional polycystin-1 dosage governs autosomal dominant polycystic kidney disease severity. *The Journal of clinical investigation.* 2012;122(11):4257-73.
50. Jin X, Muntean BS, Aal-Aaboda MS, Duan Q, Zhou J, and Nauli SM. L-type calcium channel modulates cystic kidney phenotype. *Biochim Biophys Acta.* 2014;1842(9):1518-26.
51. Liu X, Vien T, Duan J, Sheu SH, DeCaen PG, and Clapham DE. Polycystin-2 is an essential ion channel subunit in the primary cilium of the renal collecting duct epithelium. *eLife.* 2018;7.
52. Keeling J, Tsiokas L, and Maskey D. Cellular Mechanisms of Ciliary Length Control. *Cells.* 2016;5(1).
53. Piontek K, Menezes LF, Garcia-Gonzalez MA, Huso DL, and Germino GG. A critical developmental switch defines the kinetics of kidney cyst formation after loss of Pkd1. *Nat Med.* 2007;13(12):1490-5.
54. Li Y, Tian X, Ma M, Jerman S, Kong S, Somlo S, et al. Deletion of ADP Ribosylation Factor-Like GTPase 13B Leads to Kidney Cysts. *J Am Soc Nephrol.* 2016;27(12):3628-38.
55. Wann AK, and Knight MM. Primary cilia elongation in response to interleukin-1 mediates the inflammatory response. *Cellular and molecular life sciences : CMLS.* 2012;69(17):2967-77.
56. Verghese E, Ricardo SD, Weidenfeld R, Zhuang J, Hill PA, Langham RG, et al. Renal primary cilia lengthen after acute tubular necrosis. *Journal of the American Society of Nephrology : JASN.* 2009;20(10):2147-53.
57. Gallage S, and Gil J. Primary cilia and senescence: a sensitive issue. *Cell Cycle.* 2014;13(17):2653-4.
58. Pitaval A, Tseng Q, Bornens M, and Thery M. Cell shape and contractility regulate ciliogenesis in cell cycle-arrested cells. *J Cell Biol.* 2010;191(2):303-12.
59. Jackson PK. Do cilia put brakes on the cell cycle? *Nat Cell Biol.* 2011;13(4):340-2.

60. Feng Y, LoGrasso PV, Defert O, and Li R. Rho Kinase (ROCK) Inhibitors and Their Therapeutic Potential. *J Med Chem.* 2016;59(6):2269-300.
61. Parker E, Newby LJ, Sharpe CC, Rossetti S, Streets AJ, Harris PC, et al. Hyperproliferation of PKD1 cystic cells is induced by insulin-like growth factor-1 activation of the Ras/Raf signalling system. *Kidney Int.* 2007;72(2):157-65.
62. Streets AJ, Magayr TA, Huang L, Vergoz L, Rossetti S, Simms RJ, et al. Parallel microarray profiling identifies ErbB4 as a determinant of cyst growth in ADPKD and a prognostic biomarker for disease progression. *Am J Physiol Renal Physiol.* 2017;312(4):F577-F88.
63. Racusen LC, Wilson PD, Hartz PA, Fivush BA, and Burrow CR. Renal proximal tubular epithelium from patients with nephropathic cystinosis: immortalized cell lines as in vitro model systems. *Kidney Int.* 1995;48(2):536-43.
64. Ran FA, Hsu PD, Wright J, Agarwala V, Scott DA, and Zhang F. Genome engineering using the CRISPR-Cas9 system. *Nat Protoc.* 2013;8(11):2281-308.
65. Ong AC, Harris PC, Davies DR, Pritchard L, Rossetti S, Biddolph S, et al. Polycystin-1 expression in PKD1, early-onset PKD1, and TSC2/PKD1 cystic tissue. *Kidney Int.* 1999;56(4):1324-33.
66. Streets AJ, Wessely O, Peters DJ, and Ong AC. Hyperphosphorylation of polycystin-2 at a critical residue in disease reveals an essential role for polycystin-1-regulated dephosphorylation. *Human molecular genetics.* 2013;22(10):1924-39.
67. Newby LJ, Streets AJ, Zhao Y, Harris PC, Ward CJ, and Ong AC. Identification, characterization, and localization of a novel kidney polycystin-1-polycystin-2 complex. *J Biol Chem.* 2002;277(23):20763-73.
68. Gillingham AK, and Munro S. The PACT domain, a conserved centrosomal targeting motif in the coiled-coil proteins AKAP450 and pericentrin. *EMBO Rep.* 2000;1(6):524-9.
69. Kim DI, Jensen SC, Noble KA, Kc B, Roux KH, Motamedchaboki K, et al. An improved smaller biotin ligase for BioID proximity labeling. *Mol Biol Cell.* 2016;27(8):1188-96.
70. Gainullin VG, Hopp K, Ward CJ, Hommerding CJ, and Harris PC. Polycystin-1 maturation requires polycystin-2 in a dose-dependent manner. *J Clin Invest.* 2015;125(2):607-20.
71. Inoue T, Heo WD, Grimley JS, Wandless TJ, and Meyer T. An inducible translocation strategy to rapidly activate and inhibit small GTPase signaling pathways. *Nat Methods.* 2005;2(6):415-8.
72. Cebotaru L, Liu Q, Yanda MK, Boinot C, Outeda P, Huso DL, et al. Inhibition of histone deacetylase 6 activity reduces cyst growth in polycystic kidney disease. *Kidney Int.* 2016;90(1):90-9.

Figure legends

Figure 1. The ADPKD cellular phenotype is associated with structural changes in actin organisation and reduced cilia length

(A) Phalloidin labelled F-actin showing a more disorganised actin cytoskeleton in *PKD1* cystic cells (OX161) compared to control (UCL93) cells. **(B, C)** The length of actin filaments was significantly reduced and their normal parallel orientation more variable in *PKD1* compared to control cells (N=60 cells Significance determined by two-tailed students t-test). **(D)** Structured illumination (3D-SIM) confocal images of phalloidin stained cells. Actin fibres can be seen predominantly orientated to the base of control UCL93 cells. In contrast, actin fibres were thicker and frequently localised to the apical surface of OX161 cells. Increased stress fibres were also present. Cilia labelled with Arl13b (green, arrows) are shorter. **(E)** Primary cilia were visualised in quiescent control and ADPKD cell lines after serum starvation by immunofluorescence labelling of Arl13b (red) and nuclei (blue). **(F)** Cilia length was significantly reduced in a panel of human *PKD1* cystic compared to non-cystic cell lines (n=8, N=250 cells. Significance determined by one-way Anova corrected (Tukey) for multiple comparison). *p<0.05, **p<0.01, ***p<0.001, ****p<0.0001.

Figure 2. Primary cilia length correlates with PC1 expression, actin polymerisation and ROCK activity

(A) Cytochalasin D (1μM, 4h) was associated with a significant increase in cilia length in both control (UCL93) and ADPKD (OX161) lines (n=4, N=115 cells). **(B)** The ROCK inhibitor Y-27632 (1μM, 4h) rescued the cilia length defect in the ADPKD (OX161) line but had no effect on cilia length in control (UCL93) cells (n=4, N=264 cells). **(C)** Isogenic *PKD1* null cells were generated by CRISPR/Cas9 in the parental control line, UCL93. PC1 null clones (c1-3) were expanded for study. **(D)** Primary cilia were visualised in quiescent control (UCL93) and *PKD1* null lines (PC1KO) after serum starvation by immunofluorescence labelling of Arl13b (green) and nuclei (blue). **(E)** Cilia length was significantly reduced in *PKD1* null lines (PC1KO) compared to control (UCL93) cells (n=3, N=67 cells). **(F)** Expression of mCherry-PC1, mCherry-PC1-4211X or CFP-PC2 in transfected HEK293 cells showing bands of the expected size by immunoblotting for PC1 (7e12) or PC2 (G20). **(G)** Representative images of primary cilia in UCL93 control cells and OX161 cystic cells showing partial rescue of cilia length (Arl13b, green) in cells co-transfected with mCherry-PC1 (red) and CFP-PC2 but not mCherry-PC1-4211X (red) and CFP-PC2. **(H)** Expression of mCherry-PC1 was associated with a significant increase in cilia length compared to mCherry-PC1 4211X or pcDNA3 transfected control OX161 cells (n=3, N=264 cells). **** p<0.0001. Significance determined by two-tailed students t-test (A, B). Significance determined by one-way Anova corrected (Dunnett) for multiple comparison (E, H)

Figure 3. Total and centrosomal RhoA and ROCK activity is increased in ADPKD models and regulates cilia length

(A) GTP-RhoA was significantly increased in *PKD1* cystic cell lines compared to control cells (n=4) using a Rhotekin-GTP pulldown assay. **(B)** GTP-RhoA was significantly increased in *Pkd1* knockout kidneys compared to controls (n=3). **(C)** Phosphorylation of myosin light chain (pMLC), a major downstream target of ROCK, was significantly upregulated in isogenic *PKD1*

null cells (n=3). **(D)** Expression of dominant negative RhoA (T19N) in *PKD1* cells resulted in a significant increase in cilia length compared to dominant negative Cdc42 (N17) or Rac1 (N17) (n=3, N=81 cells). **(E)** Active RhoA was localised using a GTP-RhoA biosensor (R-GBD) in control and *PKD1* cells. In ciliated cells, active RhoA (GFP) was visualised at the cilia base (arrows) and was significantly increased in *PKD1* cells (n=3, N=22 cells). Insets show cilia under higher magnification (1000X magnification). **(F)** Rapamycin-inducible centrosomal targeted expression (arrow) of constitutively active RhoA (Q63L) was associated with a significant decrease in cilia length in control cells compared to uninduced cells (n=3, N=70 cells) *p<0.05, **p<0.01, ****p<0.0001. Significance determined by two-tailed students t-test (A, B, C, E). Significance determined by one-way Anova corrected (Dunnett) for multiple comparison (D, F).

Figure 4. Centrosomal ARHGAP35 localisation is regulated by PC1

(A) Candidate centrosomal ARHGAP proteins identified from cilia/centrosome databases and siRNA cilia screens. Six potential ARHGAPs were reported in at least two studies. **(B,C)** SiRNA knockdown in control cells (UCL93) demonstrated that reduced ARHGAP5, 29 and 35 expression resulted in a reduction of the percentage of ciliated cells and cilia length while knockdown of ARHGAP 1, 19 and 21 was neutral for ciliogenesis (n=3, N=50 cells). **(D)** Centrosomal expression of endogenous ARHGAP35 in HEK293 cells was demonstrated using a proximity ligation assay with a myc-tagged BioID2-PACT fusion protein (BioID2-PACT) which localises to centrosomes. In addition, endogenous ARHGAP35 was labelled by a second myc-tagged BioID2 fusion protein containing the C-terminus of PC1 (BioID2-CT1) indicating that both proteins are likely interaction partners. **(E, F)** There was reduced centrosomal expression of ARHGAP35 in *PKD1* cystic (OX161) or null (c1, c2) cells compared to control (UCL93) cells in the proximity ligation assay using BioID-PACT (n=3). *p<0.05, **p<0.01, ***p<0.001, ****p<0.0001. Significance determined by two-tailed students t-test (F). Significance determined by one-way Anova corrected (Dunnett) for multiple comparison (B, C).

Figure 5. Centrosomal ARHGAP35 interacts with PC1

(A-C) Centrosomal ARHGAP35 expression was visualised by co-localisation with γ-tubulin and labelling with a specific ARHGAP35 antibody: a clear reduction in centrosomal labelling was observed in *PKD1* null cells compared to controls. Representative images showing ARHGAP35 and γ-tubulin staining in control (A) and *PKD1* null cells (B). Staining intensity in the defined area of the centrosome was quantified by ImageJ (C) in three independent *PKD1* null clones (c1-3) compared to control cells (UCL93) (n=3, N=51 cells). **(D)** Co-expressed full-length FLAG-ARHGAP35 and V5-PC1 proteins co-immunoprecipitate in HEK293 cells indicate their likely interaction. (E) GST-pull down of FLAG-ARHGAP35 with GST-CT1 but not GST-CT1-R4227X indicates the PC1 C-terminus as the likely interaction domain. Representative blots from three independent experiments. *p<0.05, **p<0.01, ***p<0.001, ****p<0.0001. Significance determined by two-tailed students t-test . (F) schematic diagram of the expression constructs used for PC1 and ARHGAP35 experiments.

Figure 6. ROCK inhibition reduces cyst growth in vitro and in vivo

(A) The ROCK inhibitor hydroxyfasudil reduced cyst growth of a patient-derived *PKD1* cystic line (OX161) in 3D cyst assays. Representative images of cysts after 12d treatment. Average cyst area was reduced at all concentrations (1, 10, 30 μM) tested (n=3, N=96 cysts). **(B)** Hydroxyfasudil-treated *Pkd1* mice (10mg/kg/day by IP injections from PN16) (n=7) showed similar weight gain to vehicle (dH_20)-injected control animals before (n=5) and after treatment for 7d (PN22). Significance determined by one-way Anova test. **(C-E)** Hydroxyfasudil treatment was associated with a reduction in kidney size, fractional weight (2KW/BW) and cyst formation (cystic index). *p<0.05, **p<0.01, ***p<0.001, ****p<0.0001. Significance determined by two-tailed students t-test (D, E). Significance determined by one-way Anova corrected (Dunnett) for multiple comparison (A)

Figure 7. Changes in cell proliferation and cilia length in *Pkd1* mice following hydroxyfasudil treatment

(A-D) The proliferation index (Ki67) was significantly reduced (A, B) and cilia length (Arl13b) significantly increased (C, D) in hydroxyfasudil-treated animals (50 cilia per animal). **(E)** Representative images of primary cilia in *Pkd1*$^{-/-}$ kidney tissue. DBA lectin positive collecting duct cysts were stained green and primary cilia (Arl13b) labelled red. Dotted lined boxes show the region under higher magnification (1000X magnification). Mean cilia length was significantly increased in DBA positive cysts following hydroxyfasudil treatment (n=3, N=276 cells). *p<0.05, ***p<0.001, ****p<0.0001. Significance determined by two-tailed students t-test.

Figure 8. Mislocalisation of centrosomal ARHGAP35 due to PC1 mutation leads to accumulation of active RhoA, ROCK activation, increased actin polymerisation and shorter cilia in ADPKD

A model showing how mutation of PC1 could lead to reduced cilia/centrosomal localisation or retention of ARHGAP35. Two possible scenarios are shown: (1) trafficking and delivery of PC1 and ARHGAP35 in the same exocytic vesicles to the centrosome compartment and (2) retention of cleaved PC1 C-terminus (CT1) bound to centrosomal ARHGAP35. The RhoA-dependent kinase, ROCK, has been previously shown to be localised to centrosomes (32). Loss of centrosomal ARHGAP35 leads to the accumulation of centrosomal 'active' GTP-RhoA, the activation of ROCK and its downstream effectors (eg pMLC) leading to increased actin polymerisation and shorter cilia. It is plausible that the local increase in centrosomal ROCK activity could lead in turn to a cascade of ROCK activation which spreads throughout the cell.

Supplementary Figure 1

(A) The percentage of ciliated cells was reduced in ADPKD cell lines compared to controls. **(B)** Cilia length was significantly shorter in human ADPKD cystic tissue compared to control nephrectomy tissue and in **(C)** *Pkd1* cystic tissue compared to controls (n=4, N>100 cells). (**D)** The percentage of ciliated cells was significantly reduced in human ADPKD cystic tissues compared to control kidney tissues. **(E)** The percentage of ciliated cells was significantly reduced in a *Pkd1* mouse kidneys compared to wild-type littermates (n=3, N>50 cells). (**F)**

Cilia length in isogenic *PKD2* null cells generated by CRISPR/Cas9 from parental UCL93 cells was not significantly changed in five individual clones (c15, c20, c33, c37, c38) (n=3, N=20-60 cells). *p<0.05, **p<0.01, ***p<0.001, ****p<0.0001. Significance determined by two-tailed students t-test (B, C, D). Significance determined by one-way Anova corrected (Tukey) for multiple comparison (A). Significance determined by one-way Anova corrected (Dunnett) for multiple comparison (F).

Supplementary Figure 2

(A, B) GTP-bound Cdc42 and Rac-1 was quantified in ciliated control and *PKD1* cystic cells following PAK-GTP pulldown. A significant increase in GTP-Cdc42 but not GST-Rac1 was detected in *PKD1* cells compared to controls. **(C)** Positive control showing pulldown of GTP bound RhoA, Cdc42 and Rac1 following incubation with GTPγS but not with GDP. **p<0.05, **p<0.01, ***p<0.001, ****p<0.0001. Significance determined by two-tailed students t-test.

Supplementary Figure 3

(A) siRNA knockdown of candidate centrosome ARHGAPs (1, 5, 19, 21, 29, 35) in UCL93 cells validated by Taqman qPCR. **(B)** Rapamycin induced translocation of constitutively active (CA, Q63L) RhoA-FKBP-YFP fusion to the centrosome (YFP). The PACT-FRB-HA anchor fusion is targeted to centrosomes as shown by HA immunofluorescence (left panel). **(C)** Localisation of Myc-BioID2-PACT and CT1 constructs to the centrosome and plasma membrane respectively as shown by myc tag labelling. **(D)** BioID2 proximity ligation assay with centrosome-targeted BioID2-PACT and BioID2-CT1 in HEK293 cells demonstrating that ARHGAP5 and 29 are detectable at centrosomes and in close proximity to the PC1 C-terminus which is localised to centrosome and non-centrosome compartments. **(E)** Centrosomal expression of ARHGAP5 and ARHGAP29 was unchanged in *PKD1* cystic (OX161) or null (c1, c2) cells compared to control (UCL93) cells in the proximity ligation assay using BioID-PACT. *p<0.05, **p<0.01, ***p<0.001, ****p<0.0001. Significance determined by two-tailed students t-test.

Supplementary Figure 4

(A) LTA lectin staining in *Pkd1* kidney tissues shows that the majority of cysts are not derived from proximal tubular cells on this model; (**B)** BUN measurements show a small non-significant reduction in hydroxyfasudil treated animals in *Pkd1* knockout mice. No significant difference in BUN was seen between uninduced and induced *Pkd1* animals at PN23 or in uninduced mice following 7 days of hydroxyfasudil treatment. *p<0.05, **p<0.01, ***p<0.001, ****p<0.0001. Significance determined by two-tailed students t-test.

Supplementary Movies

3D rotating image of phalloidin and Arl13b stained cells generated by structured illumination (3D-SIM) microscopy and Imaris image analysis software (Bitplane). Movie 1 (control cells, UCL93); Movie 2 (*PKD1* cells, OX161).

Figure 1

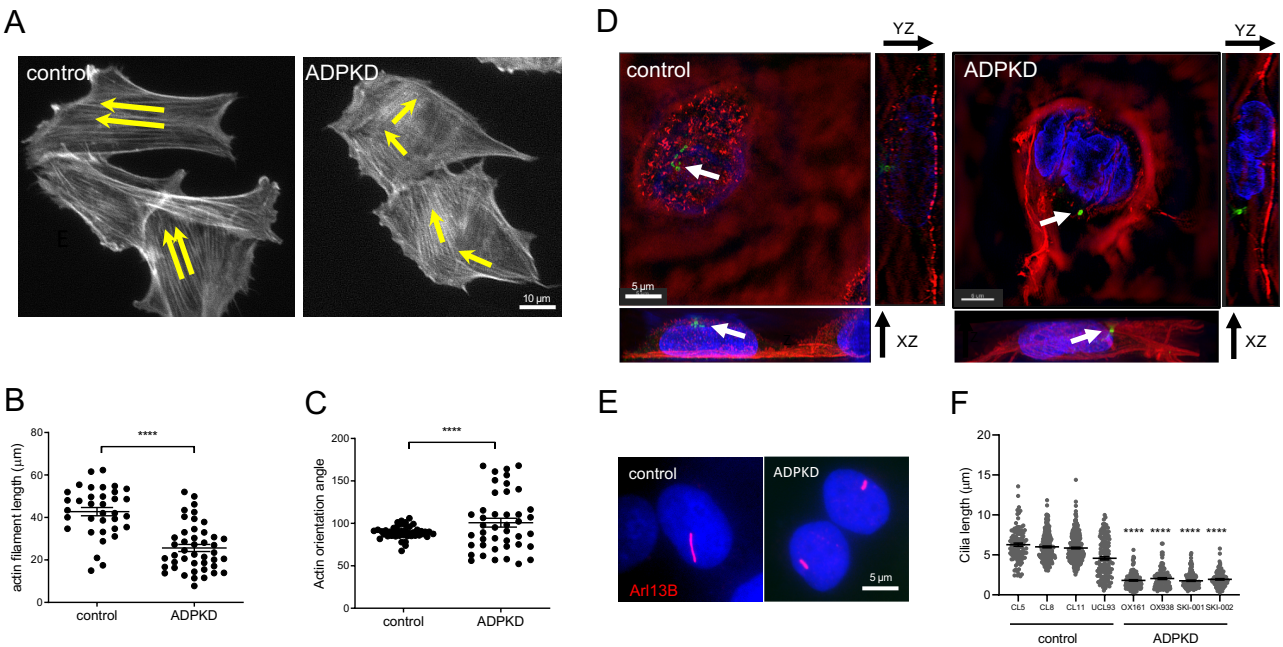
A
control
ADPKD
10 µm
D
YZ
control
ADPKD
5 µm
XZ
B
actin filament length (µm)
****
control
ADPKD
C
Actin orientation angle
****
control
ADPKD
E
control
ADPKD
Arl13B
5 µm
F
Cilia length (µm)
CL5
CL8
CL11
UCL93
OX161
OX938
SKI-001
SKI-002
****
control
ADPKD

Figure 2

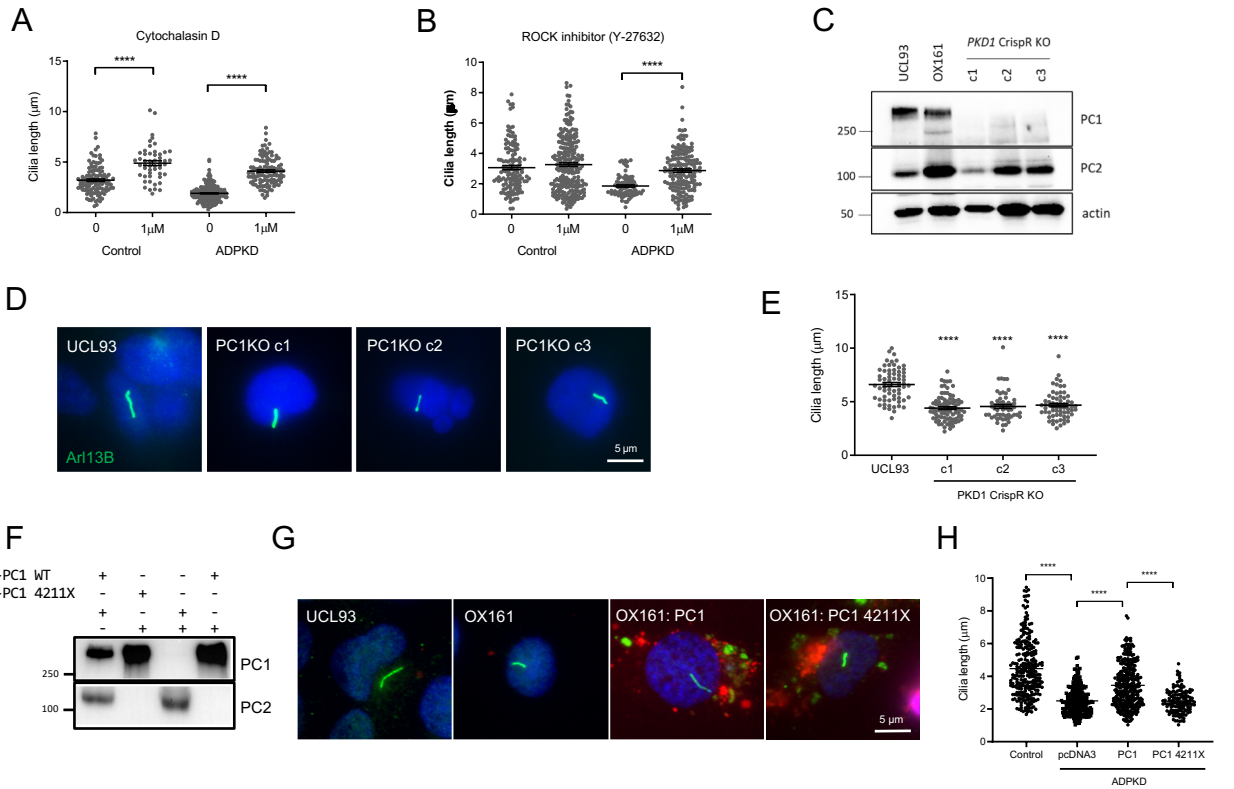
A
Cytochalasin D
Cilia length (μm)
****
****
0
1μM
0
1μM
Control
ADPKD
B
ROCK inhibitor (Y-27632)
Cilia length (μm)
****
0
1μM
0
1μM
Control
ADPKD
C
UCL93
OX161
PKD1 CrispR KO
c1
c2
c3
PC1
PC2
actin
250
100
50
D
UCL93
PC1KO c1
PC1KO c2
PC1KO c3
Arl13B
5 μm
E
Cilia length (μm)
****
****
****
UCL93
c1
c2
c3
PKD1 CrispR KO
F
mCherry-PC1 WT
mCherry-PC1 4211X
PC2
pcDNA3
PC1
PC2
250
100
G
UCL93
OX161
OX161: PC1
OX161: PC1 4211X
5 μm
H
Cilia length (μm)
****
****
****
Control
pcDNA3
PC1
PC1 4211X
ADPKD

Figure 3

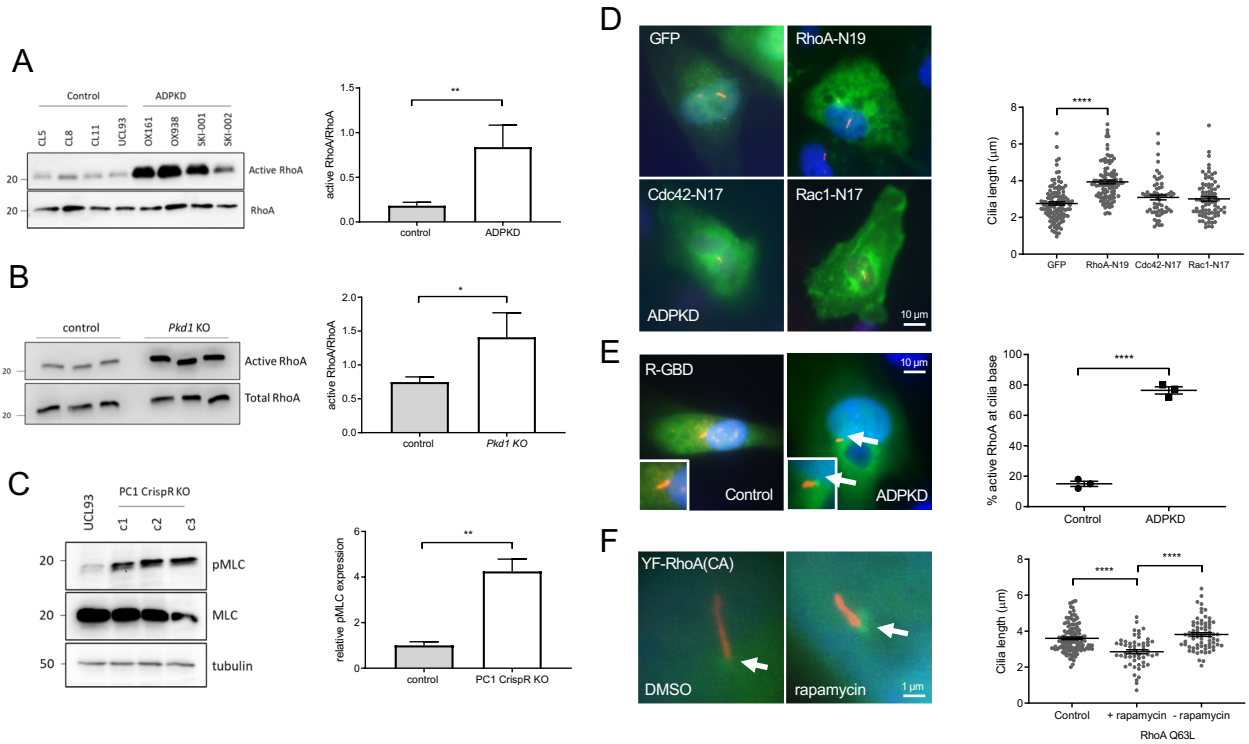
A
Control
ADPKD
CL5
CL8
CL11
UCL93
OX161
OX938
SKI-001
SKI-002
Active RhoA
RhoA
20
20
active RhoA/RhoA
control
ADPKD
B
control
Pkd1 KO
Active RhoA
Total RhoA
active RhoA/RhoA
control
Pkd1 KO
C
UCL93
PC1 CrispR KO
c1
c2
c3
pMLC
MLC
tubulin
50
relative pMLC expression
control
PC1 CrispR KO
D
GFP
RhoA-N19
Cdc42-N17
Rac1-N17
ADPKD
10 µm
Cilia length (µm)
GFP
RhoA-N19
Cdc42-N17
Rac1-N17
E
R-GBD
Control
ADPKD
10 µm
% active RhoA at cilia base
Control
ADPKD
F
YF-RhoA(CA)
DMSO
rapamycin
1 µm
Cilia length (µm)
Control
+ rapamycin
- rapamycin
RhoA Q63L

Figure 4

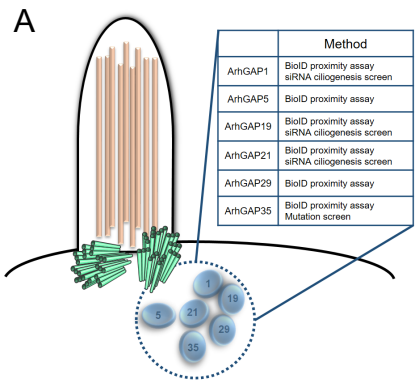
A
Method
ArhGAP1
BioID proximity assay
siRNA ciliogenesis screen
ArhGAP5
BioID proximity assay
ArhGAP19
BioID proximity assay
siRNA ciliogenesis screen
ArhGAP21
BioID proximity assay
siRNA ciliogenesis screen
ArhGAP29
BioID proximity assay
ArhGAP35
BioID proximity assay
Mutation screen
1
19
5
21
29
35

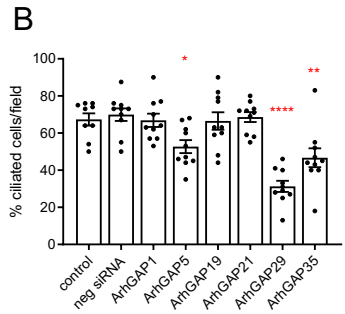
B
% ciliated cells/field
100
80
60
40
20
0
*
****
**
control
neg siRNA
ArhGAP1
ArhGAP5
ArhGAP19
ArhGAP21
ArhGAP29
ArhGAP35

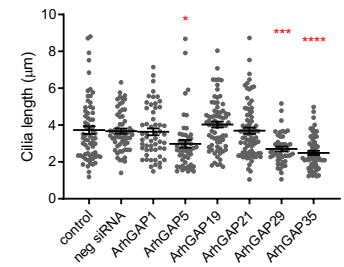
C
Cilia length (µm)
10
8
6
4
2
0
*
***
****
control
neg siRNA
ArhGAP1
ArhGAP5
ArhGAP19
ArhGAP21
ArhGAP29
ArhGAP35

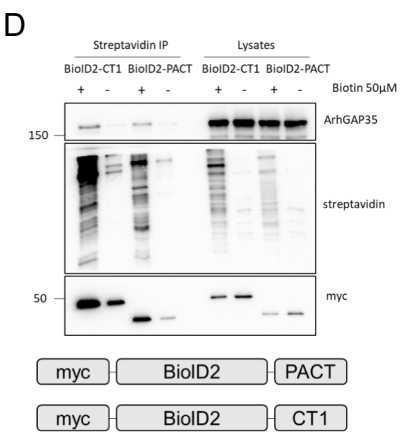
D
Streptavidin IP
Lysates
BioID2-CT1
BioID2-PACT
BioID2-CT1
BioID2-PACT
+ - + - + - + -
Biotin 50µM
150
50
ArhGAP35
streptavidin
myc
myc
BioID2
PACT
myc
BioID2
CT1

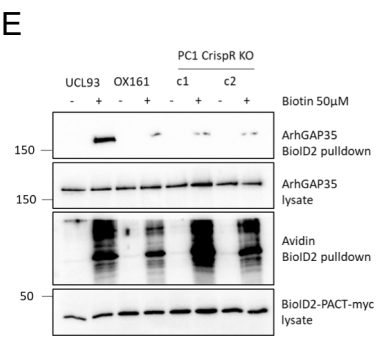
E
PC1 CrispR KO
UCL93
OX161
c1
c2
- + - + - + - +
Biotin 50µM
150
150
50
ArhGAP35
BioID2 pulldown
ArhGAP35
lysate
Avidin
BioID2 pulldown
BioID2-PACT-myc
lysate

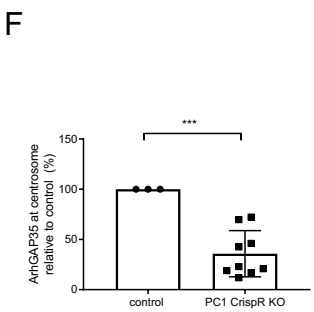
F
***
ArhGAP35 at centrosome
relative to control (%)
150
100
50
0
control
PC1 CrispR KO

Figure 5

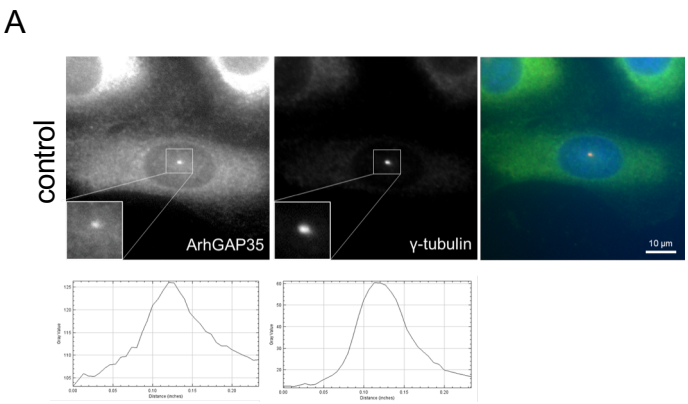
A
control
ArhGAP35
γ-tubulin
10 μm

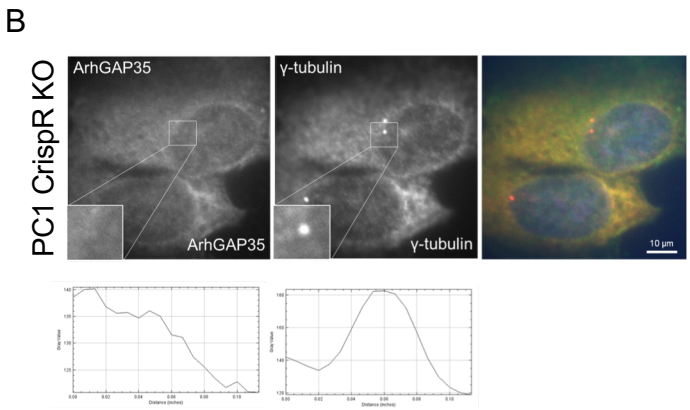
B
PC1 CrispR KO
ArhGAP35
ArhGAP35
γ-tubulin
γ-tubulin
10 μm

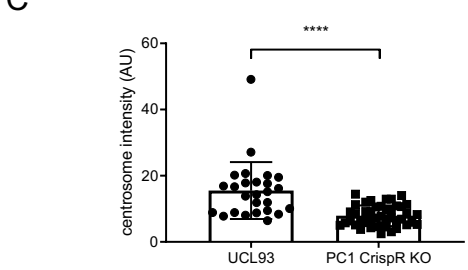
C
****
centrosome intensity (AU)
60
40
20
0
UCL93
PC1 CrispR KO

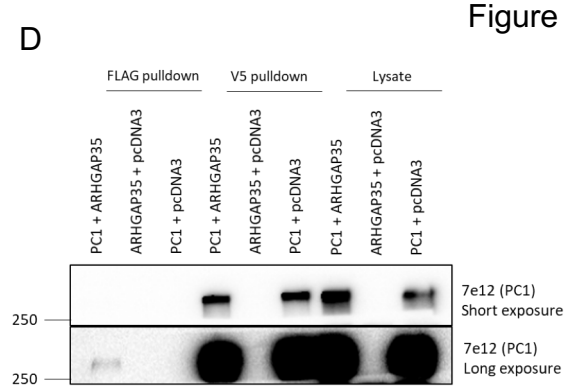
D
FLAG pulldown
V5 pulldown
Lysate
PC1 + ARHGAP35
ARHGAP35 + pcDNA3
PC1 + pcDNA3
PC1 + ARHGAP35
ARHGAP35 + pcDNA3
PC1 + pcDNA3
PC1 + ARHGAP35
ARHGAP35 + pcDNA3
PC1 + pcDNA3
250
250
7e12 (PC1)
Short exposure
7e12 (PC1)
Long exposure

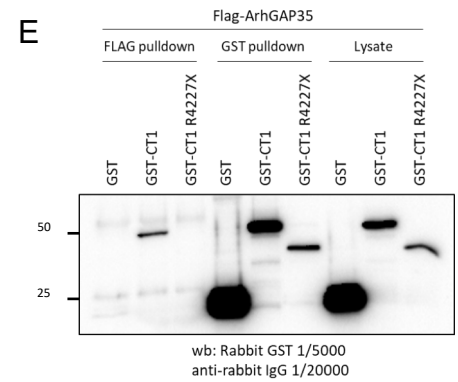
E
Flag-ArhGAP35
FLAG pulldown
GST pulldown
Lysate
GST
GST-CT1
GST-CT1 R4227X
GST
GST-CT1
GST-CT1 R4227X
GST
GST-CT1
GST-CT1 R4227X
50
25
wb: Rabbit GST 1/5000
anti-rabbit IgG 1/20000


F
V5
Polycystin-1
+
Flag
ArhGAP35
GST
CT1
+
Flag
ArhGAP35
GST
CT1-R4227X
+
Flag
ArhGAP35
GST
+
Flag
ArhGAP35

Figure 6

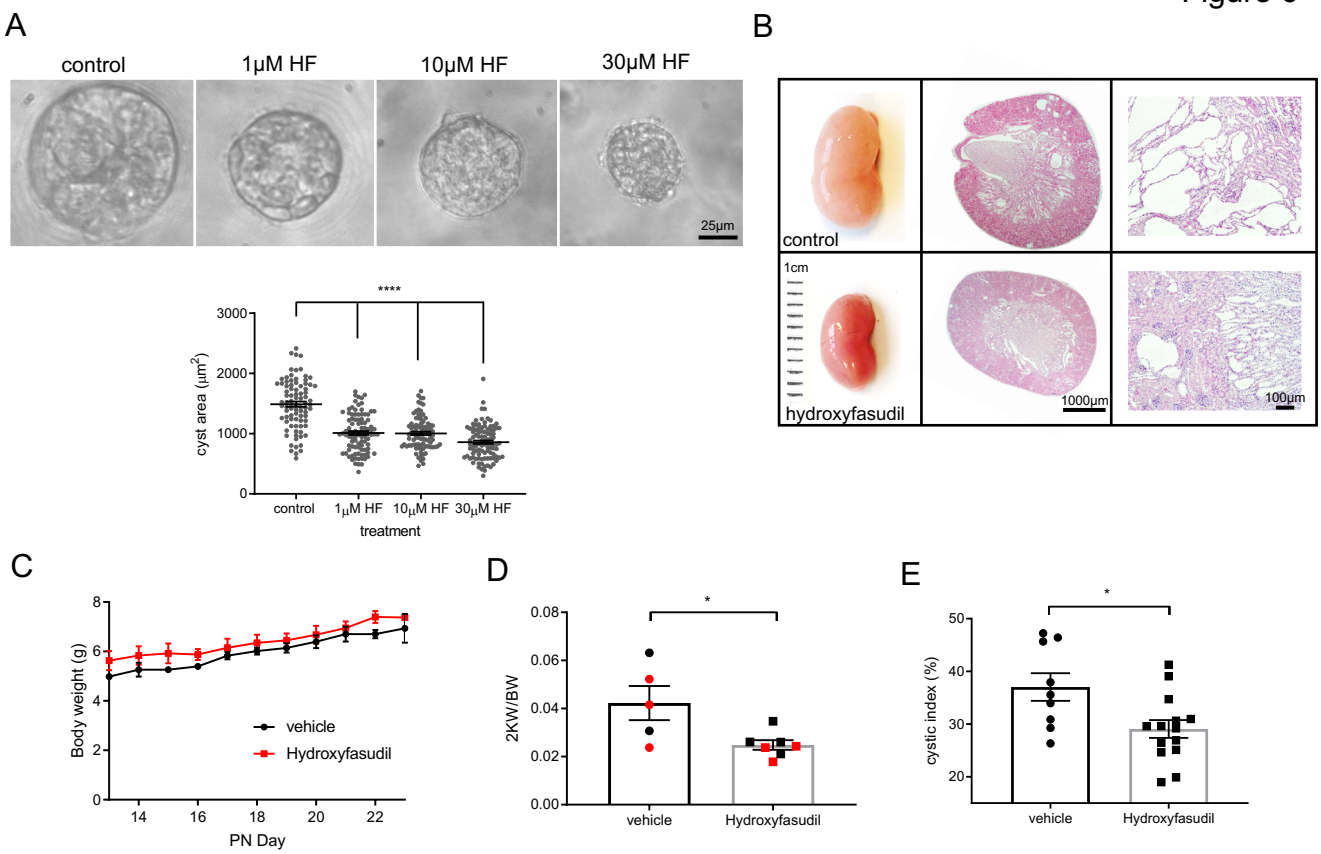
A
control
1μM HF
10μM HF
30μM HF
25μm
****
cyst area (μm²)
3000
2000
1000
0
control
1μM HF
10μM HF
30μM HF
treatment
B
control
1cm
hydroxyfasudil
1000μm
100μm
C
Body weight (g)
8
6
4
2
0
14
16
18
20
22
PN Day
vehicle
Hydroxyfasudil
D
2KW/BW
0.08
0.06
0.04
0.02
0.00
*
vehicle
Hydroxyfasudil
E
cystic index (%)
50
40
30
20
*
vehicle
Hydroxyfasudil

Figure 7

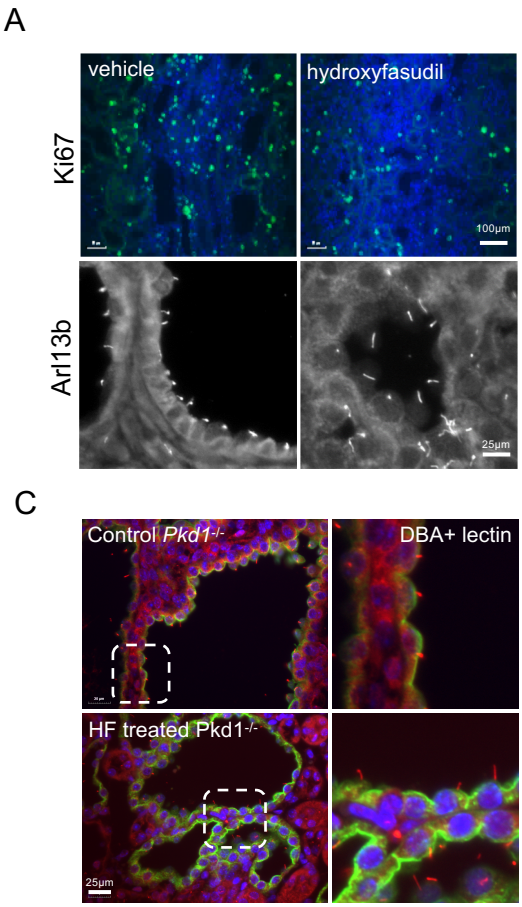
A
vehicle
hydroxyfasudil
Ki67
Arl13b
100μm
25μm
C
Control Pkd1-/-
DBA+ lectin
HF treated Pkd1-/-
25μm
B
***
Ki67 proliferation index (%)
30
20
10
0
vehicle
hydroxyfasudil
D
****
Cilia length (μm)
10
8
6
4
2
0
vehicle
hydroxyfasudil
E
****
Cilia length (μm)
10
8
6
4
2
0
controls
hydroxyfasudil

Figure 8

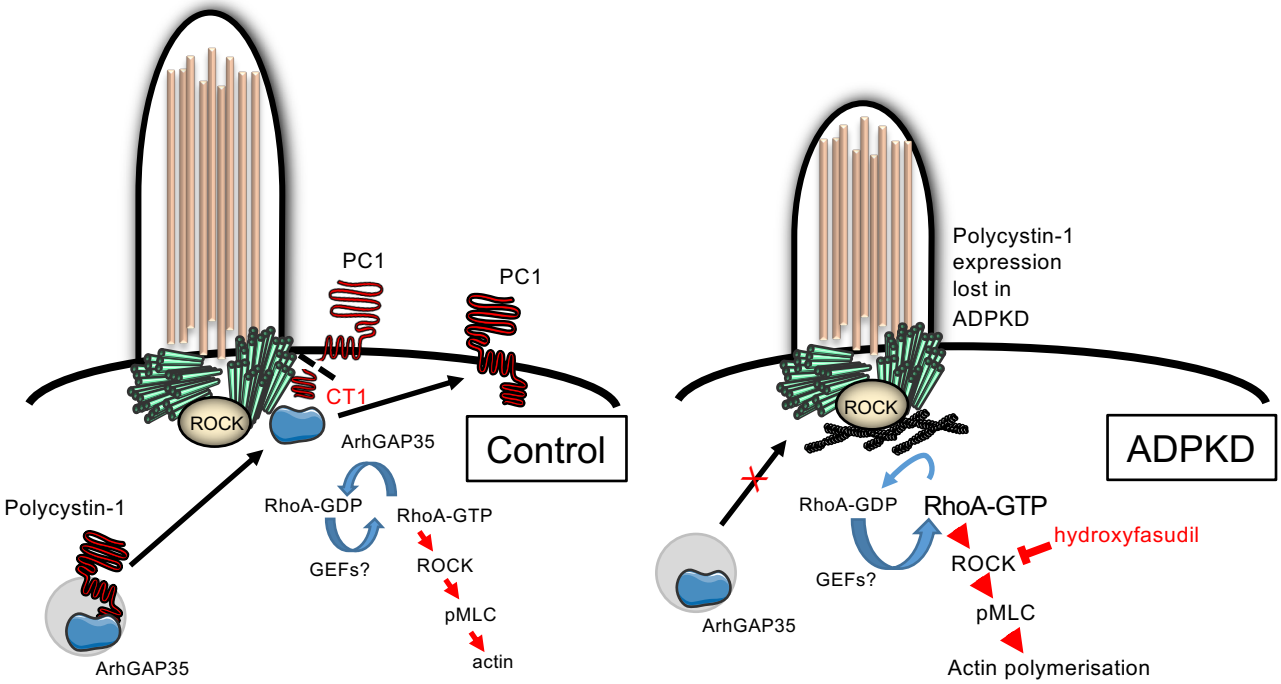
PC1
PC1
CT1
ROCK
ArhGAP35
Control
Polycystin-1
RhoA-GDP
RhoA-GTP
GEFs?
ROCK
pMLC
actin
ArhGAP35
Polycystin-1
expression
lost in
ADPKD
ROCK
ADPKD
RhoA-GDP
RhoA-GTP
hydroxyfasudil
GEFs?
ROCK
pMLC
ArhGAP35
Actin polymerisation